

On the use of the adiabatic molecular dynamics technique in the calculation of free energy profiles

Lula Rosso, Peter Mináry, and Zhongwei Zhu

Department of Chemistry, New York University, New York, New York 10003

Mark E. Tuckerman

Department of Chemistry and Courant Institute of Mathematical Sciences, New York University, New York, New York 10003

(Received 24 September 2001; accepted 12 December 2001)

A new molecular dynamics method for calculating free energy profiles for rare events is presented. The new method is based on the creation of an adiabatic separation between a reaction coordinate subspace and the remaining degrees of freedom within a molecular dynamics run. This is achieved by associating with the reaction coordinate(s) a high temperature and large mass, thereby allowing the activated process to occur while permitting the remaining degrees of freedom to respond adiabatically. In this limit, by applying a formal multiple time scale Liouville operator factorization, it can be rigorously shown that the free energy profile is obtained directly from the probability distribution of the reaction coordinate subspace and, therefore, no unbiasing of the configuration space or postprocessing of the output data is required. The new method is applied to a variety of model problems including a two-dimensional free energy surface and its performance tested against free energy calculations using the “blue moon ensemble” approach. The comparison shows that free energy profiles can be calculated with greater ease and efficiency using the new method. © 2002 American Institute of Physics. [DOI: 10.1063/1.1448491]

I. INTRODUCTION

One of the most important quantities in thermodynamics is the reversible work needed to change the thermodynamic state of a system. Under certain conditions, this quantity will be independent of the path taken between the initial and final states and will, therefore, be related to the free energy difference between these two states. As a result, considerable effort has been invested in the development of methods to compute such free energy differences (see, e.g., Ref. 1 for a review and comparison). A problem that is frequently encountered is that of computing the free energy profile along a reaction path on a potential energy surface characterized by a reaction coordinate q . Not only does the free energy profile provide a thermodynamic picture along the reaction path, but it also permits determination of activation energies and estimation of associated rate constants via classical or quantum transition state theory. In many instances, a multidimensional free energy profile or surface characterized by a set of reaction coordinates may be of particular interest. The ability to characterize a process by a reaction coordinate or coordinates generally assumes some prior knowledge of the process under consideration. Clearly, such a well defined reaction coordinate subspace is not always available, in which case, it may be appropriate to apply methods such as the recently introduced transition path sampling technique.^{2–4} However, identification of a useful reaction coordinate or coordinates is often possible, and, therefore, novel and efficient methods for computing profiles along these coordinates are desirable.

It should be noted that the present class of free energy calculations differs somewhat from other types, such as solvation or binding free energy calculations, wherein a system

is transformed between two thermodynamic states characterized by different potentials, usually by introducing a variable coupling parameter (see, for example, Refs. 5–11). Although some similarities exist between these two classes of free energy calculations, there are different technical issues associated with each type, and a variety of effective methods have been developed to treat this latter case^{5–10} (see, in particular, the work of Warshel and co-workers^{5,6,11} for a discussion of novel empirical valence bond based approaches). Indeed, we expect that the methodology to be presented herein could be easily adapted for and combined with methods for treating this latter type of free energy calculation, however, further comments on this notion will be deferred until the conclusion section.

Statistical mechanics provides a means whereby such free energy profiles can be determined directly from ensemble averages. In the case of a classical N -particle system at temperature T , a reaction coordinate q is expressible as a function $q = q(\mathbf{r}_1, \dots, \mathbf{r}_N)$ of the N Cartesian position vectors $\{\mathbf{r}_1, \dots, \mathbf{r}_N\}$ of the N particles. The free energy profile, $F(q')$, is then defined by

$$F(q') = -\frac{1}{\beta} \ln P(q'), \quad (1)$$

where

$$P(q') = \langle \delta(q(\mathbf{r}_1, \dots, \mathbf{r}_N) - q') \rangle \quad (2)$$

is the probability density for the reaction coordinate to take on the value q' and $\beta = 1/kT$. Analogous formulas hold for multidimensional free energy profiles. In principle, the probability distribution in Eq. (2) can be computed directly from

a molecular dynamics (MD) or Monte Carlo simulation. However, if the reaction path described by q corresponds to a rare event with a high activation energy, then the use of direct simulation techniques is infeasible due to the presence of very low probability regions in the configuration space. Consequently special techniques such as umbrella sampling,^{12–14} thermodynamic integration in conjunction with the so-called “blue moon ensemble” method,^{15,16} guiding potentials,^{17,18} nonequilibrium techniques,¹⁹ projection methods,²⁰ and variable transformation approaches²¹ have been developed. With the exception of the latter two, these approaches do not directly yield the probability distribution in Eq. (2). Rather, they are based on the introduction of a bias on the configuration space which artificially drives the system into low probability regions. Averages must, then, be performed by applying appropriate unbiasing factors or reweighting procedures. In addition, the umbrella and blue moon methods, which use restraints/constraints to bias the phase space, require that separate simulations be performed at each value of the reaction coordinate and that weighted histogram²² or thermodynamic integration methods be applied in order to construct the free energy profile. Despite the enhancement of sampling efficiency caused by the bias, free energy calculations remain computationally very intensive and relatively complex to perform.

In this paper, an alternative approach to the calculation of free energy profiles along reaction paths is presented. We have already laid the groundwork for this method in Ref. 23. The new method, which will be shown to yield the probability distribution function in Eq. (2) directly, is based on the creation of a dynamical adiabatic separation between the reaction coordinate and remaining degrees of freedom.²³ In particular, a dynamical scheme is constructed in which the reaction coordinate evolves slowly relative to the other degrees of freedom and is simultaneously maintained at a high temperature. The latter condition, which has also been employed on entire molecules by other authors to enhance sampling of configuration space,^{24,25} ensures that all activation barriers along the reaction path can be easily crossed and can be enforced by coupling the reaction coordinate to its own heat bath or thermostat. The former condition permits the remaining degrees of freedom to fully relax in response to the motion of the reaction coordinate and, thereby, sample a large portion of their configuration space as the reaction coordinate slowly evolves. Indeed, adiabatic dynamics methods have been employed successfully to perform approximate quantum dynamics simulations^{26,27} as well as Car–Parrinello-type *ab initio* molecular dynamics.²⁸ A careful analysis of the resulting dynamics (see Sec. II) reveals that the free energy profile will then be given by Eq. (1) with β replaced by $\beta_q = 1/kT_q$, where T_q is the temperature of the reaction coordinate (see Sec. II). It is then clear that the use of such an approach eliminates all biasing from the simulation procedure and, hence, the need for postprocessing of the output data. It is also found that the new adiabatic free energy dynamics (AFED) method allows the free energy profile to be determined with greater efficiency than constrained/restrained methods such as the blue moon and umbrella sampling schemes.

We note, here, that we have recently introduced a variable transformation scheme for enhancing conformational sampling²¹ that can also yield free energy profiles. This approach, while very effective, requires knowledge of specific features of the potential surface. This information may not always be available as, for example, when complex reaction coordinates are used or in *ab initio* molecular dynamics calculations. Therefore, alternative methods are desirable. The present adiabatic method, by contrast, requires no specific information about the potential and, therefore, is more generally applicable.

This paper is organized as follows: In Sec. II, the adiabatic dynamics method is analyzed in detail and shown to yield the free energy profile directly from Eq. (1) with β replaced by β_q . The analysis is based on the use of the Liouville operator technique and a formally exact multiple time scale breakup of the adiabatic classical propagator. In Sec. III, several model problems are examined using the new approach. In these examples, direct comparison to analytical solutions (when available) and the blue moon ensemble method are made. In Sec. IV, a discussion and procedure for setting up adiabatic conditions for a given problem are presented. Conclusions and prospects for extending this work to more complex situations, other types of free energy calculations, and quantum free energy profiles are discussed in Sec. V.

II. THEORETICAL ANALYSIS OF THE ADIABATIC DYNAMICS APPROACH

In order to illustrate the method, we consider a simple model system, which serves as a paradigm for the general problem of determining free energy profiles. The model consists of two degrees of freedom, namely, a reaction coordinate x with mass m_x and an additional degree of freedom y with mass m_y . The two degrees of freedom are coupled through a potential $V(x,y)$, and the Hamiltonian of the system is taken to be of the form,

$$H = \frac{p_x^2}{2m_x} + \frac{p_y^2}{2m_y} + V(x,y). \quad (3)$$

The simple analysis based on Eq. (3) neglects the fact that, in generalized coordinates, the kinetic energy will actually involve a (generally) coordinate-dependent mass metric tensor. An analysis and procedure for circumventing such difficulties in treating N -particle systems in terms of generalized coordinates is given in Appendix A.

If ω_x and ω_y are characteristic frequencies of the x and y motion, then an adiabatic separation between x and y is achieved by requiring that $\omega_x \ll \omega_y$. This can be realized dynamically by choosing the masses such that $m_x \gg m_y$. In addition, temperatures T_x and T_y associated with the two degrees of freedom are introduced such that $T_x \gg T_y$, as noted above. The latter condition allows x to easily cross barriers along the reaction path. In the preceding discussion, a detailed analysis of the dynamics and the phase space it generates will be carried out. The goal of this analysis is to show that, under the usual assumptions of ergodicity, the

resulting phase space distribution function of the reaction coordinate, x , leads to a free energy profile given by Eq. (1) with β replaced by $\beta_x = 1/kT_x$.

In order to maintain the two temperatures, T_x and T_y in the system, the dynamics generated by Eq. (3) must be supplemented by coupling the variables x and y to independent heat baths or thermostats. Thus, the phase space evolution of the system is governed by a Liouville operator of the form,

$$iL = \frac{p_x}{m_x} \frac{\partial}{\partial x} + \frac{p_y}{m_y} \frac{\partial}{\partial y} + F_x \frac{\partial}{\partial p_x} + F_y \frac{\partial}{\partial p_y} + iL_{\text{therm}}^{(x)}(T_x) + iL_{\text{therm}}^{(y)}(T_y), \quad (4)$$

where $F_x = -\partial V/\partial x$, $F_y = -\partial V/\partial y$ and $iL_{\text{therm}}^{(x)}(T_x)$ and $iL_{\text{therm}}^{(y)}(T_y)$ are dynamical thermostats, e.g., the Nosé–Hoover chain (NHC),²⁹ or the recently introduced generalized Gaussian moment thermostat (GGMT),³⁰ which maintain x at temperature T_x and y at temperature T_y . The explicit forms of the thermostat operators are not important for the present discussion, however, the interested reader is referred to Refs. 29 and 30 for the detailed expressions of these operators. For the present discussion, it is sufficient to know that they act on the momenta p_x and p_y in such a way as to control the kinetic energy fluctuations and generate a Maxwell–Boltzmann distribution in these variables at the required temperatures and that they involve a set of additional or “extended” phase space variables, denoted generally by $\Gamma_{\text{therm},x}$ and $\Gamma_{\text{therm},y}$. It is, again, stressed that two separate thermostats are needed in order to maintain the two separate temperatures T_x and T_y .

The time evolution of the full phase space vector, $\Gamma = \{x, y, p_x, p_y, \Gamma_{\text{therm},x}, \Gamma_{\text{therm},y}\}$, starting from an initial condition $\Gamma(0)$, is formally given by

$$\Gamma(t) = e^{iL t} \Gamma(0), \quad (5)$$

where $\exp(iL t)$ is the classical propagator. Consider the evolution of the system over a time interval Δt characteristic of the x motion. In order to analyze the dynamics over such an interval, it is useful to define “reference system” Liouville operators,

$$iL_{\text{ref}}^{(x)}(T_x) = \frac{p_x}{m_x} \frac{\partial}{\partial x} + iL_{\text{therm}}^{(x)}(T_x), \quad (6)$$

$$iL_{\text{ref}}^{(y)}(T_y) = \frac{p_y}{m_y} \frac{\partial}{\partial y} + iL_{\text{therm}}^{(y)}(T_y),$$

and express the total Liouville operator as

$$iL = iL^{(y)} + iL_{\text{ref}}^{(x)}, \quad (7)$$

where

$$iL^{(y)} = iL_{\text{ref}}^{(y)} + F_y \frac{\partial}{\partial p_y} + F_x \frac{\partial}{\partial p_x}. \quad (8)$$

Using the Trotter theorem, a reversible, symplectic factorization of the classical propagator is constructed according to

$$\exp(iL \Delta t) = \exp\left(iL^{(y)} \frac{\Delta t}{2}\right) \exp(iL_{\text{ref}}^{(x)} \Delta t) \exp\left(iL^{(y)} \frac{\Delta t}{2}\right). \quad (9)$$

In Eq. (9), note that the y -propagator, $\exp(iL^{(y)} \Delta t/2)$, is left intact. The factorization scheme in Eq. (9) allows the y -propagator to be evaluated formally exactly, again, using the Trotter theorem,

$$\begin{aligned} \exp\left(iL^{(y)} \frac{\Delta t}{2}\right) &= \lim_{n \rightarrow \infty} \left[\exp\left(\frac{\Delta t}{4n} F_x \frac{\partial}{\partial p_x}\right) \right. \\ &\times \exp\left(\frac{\Delta t}{4n} F_y \frac{\partial}{\partial p_y}\right) \exp\left(iL_{\text{ref}}^{(y)} \frac{\Delta t}{2n}\right) \\ &\times \exp\left(\frac{\Delta t}{4n} F_y \frac{\partial}{\partial p_y}\right) \exp\left(\frac{\Delta t}{4n} F_x \frac{\partial}{\partial p_x}\right) \left. \right]^n. \end{aligned} \quad (10)$$

When Eq. (10) is substituted into Eq. (9), the result is the formally exact analog of a multiple time scale factorization such as is discussed in Ref. 31. The formally exact evaluation of the y -propagator is necessary since, under the adiabatic conditions of the problem, the time interval, Δt , is very long compared to the time scale on which y evolves. Combining Eqs. (9) and (10) and acting with the resulting operator on the full phase space vector $\Gamma(0)$ yields the following evolution of the physical variables:^{25,27}

$$\begin{aligned} x(\Delta t) &= x_{\text{ref}}[x(0), \dot{x}(\Delta t/2), \Gamma_x(0); \Delta t], \\ \dot{x}(\Delta t) &= \dot{x}_{\text{ref}}[x(0), \dot{x}(\Delta t/2), \Gamma_x(0); \Delta t] \\ &\quad + \frac{1}{m_x} \int_{\Delta t/2}^{\Delta t} dt' F_x[y_{\text{adb}}(y(\Delta t/2), \dot{y}(\Delta t/2), \\ &\quad \Gamma_y(\Delta t/2), x(\Delta t); t'), x(\Delta t)], \\ \dot{x}(\Delta t/2) &= \dot{x}(0) + \frac{1}{m_x} \int_0^{\Delta t/2} dt' F_x[y_{\text{adb}}(y(0), \dot{y}(0), \\ &\quad \Gamma_y(0), x(0); t'), x(0)], \\ y(\Delta t/2) &= y_{\text{adb}}[y(0), \dot{y}(0), \Gamma_y(0), x(0); \Delta t/2], \quad (11) \\ \dot{y}(\Delta t/2) &= \dot{y}_{\text{adb}}[y(0), \dot{y}(0), \Gamma_y(0), x(0); \Delta t/2], \\ y(\Delta t) &= y_{\text{adb}}[y(\Delta t/2), \dot{y}(\Delta t/2), \Gamma_y(\Delta t/2), x(\Delta t); \Delta t], \\ \dot{y}(\Delta t) &= \dot{y}_{\text{adb}}[y(\Delta t/2), \dot{y}(\Delta t/2), \Gamma_y(\Delta t/2), x(\Delta t); \Delta t], \end{aligned}$$

where $\dot{x} = p_x/m_x$ and $\dot{y} = p_y/m_y$. In Eq. (11), $x_{\text{ref}}[x', \dot{x}', \Gamma'_x; t']$ indicates the evolution of x under the action of the reference system Liouville operator $iL_{\text{ref}}^{(x)}$ up to time t' starting from initial conditions x' , \dot{x}' , and Γ'_x with an analogous meaning for $\dot{x}_{\text{ref}}[x', \dot{x}', \Gamma'_x; t']$. Similarly, $y_{\text{adb}}[y', \dot{y}', \Gamma'_y, x'; t']$ indicates the exact adiabatic, i.e., at fixed $x = x'$, evolution of y up to time t' under the action of the operator in brackets in Eq. (11) starting from initial conditions y', \dot{y}', Γ'_y . Analytical forms for these functions cannot generally be supplied, however, the analysis does not require that these functions be explicitly known. The time integrals appearing in Eqs. (11) are a direct result of the infinite product of operators in brackets in Eq. (10) which

arise from application of the Trotter theorem and which lead to the (infinite sum) limit of a trapezoidal rule expression for the integral. Since $m_x \gg m_y$, the motion of the y variable will follow instantaneously the motion of x dynamically and sample its available configuration space over the time interval $\Delta t/2$ during which x remains fixed. In Eq. (11), it can be seen that the force governing the evolution of x and \dot{x} can be related to a time average of F_x over the adiabatic y trajectory.

Assuming that the y motion is ergodic over this time interval, then the time integral of F_x appearing in Eq. (11) can be replaced by a configurational average over y at fixed x according to

$$\begin{aligned} \frac{2}{\Delta t} \int_{\tau}^{\tau+\Delta t/2} dt F_x[y_{\text{adb}}(y(\tau), \dot{y}(\tau), \Gamma_y(\tau), x; t), x] \\ = \frac{\int dy F_x(x, y) e^{-\beta_y V(x, y)}}{\int dy e^{-\beta_y V(x, y)}} = \frac{\partial}{\partial x} \frac{1}{\beta_y} \ln Z_y(x; \beta_y), \end{aligned} \quad (12)$$

where $\beta_y = 1/kT_y$ and

$$Z_y(x; \beta_y) = \int dy e^{-\beta_y V(x, y)} \quad (13)$$

is an effective configurational partition function of x . Therefore, in the adiabatic limit, an effective Hamiltonian for the x degree of freedom can be constructed according to

$$H_{x,\text{adb}}(p_x, x) = K_x - \frac{1}{\beta_y} \ln Z_y(x; \beta_y), \quad (14)$$

where $K_x = p_x^2/2m_x$. From Eq. (14) follow the statistical mechanical properties of the x degree of freedom. The partition function for x , correct in the adiabatic limit, is given by

$$\begin{aligned} Q(\beta_x; \beta_y) &= \int dp_x dx \exp(-\beta_x H_{x,\text{adb}}(p_x, x)) \\ &= \int dp_x \exp(-\beta_x K_x) \int dx \\ &\quad \times \exp\left[-\beta_x \left(-\frac{1}{\beta_y} \ln Z_y(x; \beta_y)\right)\right] \\ &= \int dp_x \exp(-\beta_x K_x) \int dx [Z_y(x; \beta_y)]^{\beta_x/\beta_y}. \end{aligned} \quad (15)$$

Therefore, the probability distribution function of x , in the adiabatic limit, becomes

$$\begin{aligned} P_{\text{adb}}(x) &= \frac{1}{Q(\beta_x, \beta_y)} \int dp_x \exp(-\beta_x K_x) \\ &\quad \times [Z_y(x; \beta_y)]^{\beta_x/\beta_y} \end{aligned} \quad (16)$$

so that $P_{\text{adb}}(x) \propto [Z_y(x; \beta_y)]^{\beta_x/\beta_y}$. From Eq. (16), it follows that the free energy profile, $F(x)$, which, by definition, is

$$F(x) = -\frac{1}{\beta_y} \ln Z_y(x; \beta_y) \quad (17)$$

can be calculated directly from the adiabatically generated probability distribution function, $P_{\text{adb}}(x)$ by

$$F(x) = -\frac{1}{\beta_x} \ln P_{\text{adb}}(x) + \text{const.} \quad (18)$$

The equivalence between Eqs. (17) and (18) can be seen by direct substitution of $P_{\text{adb}}(x)$ into Eq. (18). Thus, the true free energy profile can be obtained, up to an irrelevant constant, from the probability distribution function, $P_{\text{adb}}(x)$ generated by the adiabatic dynamics with $m_x \gg m_y$ and $T_x \gg T_y$ via Eq. (18). Note that Eq. (18) is of the same form as the standard free energy profile defined in Eq. (1) with T , the temperature of the ensemble, replaced by T_x the temperature to which the x degree of freedom has been heated. Despite the fact that T_x appears in Eq. (18), the *correct* free energy profile at the temperature, T_y of the bath/environment is obtained. Equation (18) constitutes the central result of this paper.

It should be noted that the present adiabatic dynamics approach differs from adiabatic stepwise methods, in which a free energy change as x varies from x_1 to x_2 is computed as a weighted average over a trajectory evolving on the potential $V(x_1, y)$ (for an explanation of such methods and when they fail, see, for example, Ref. 11). As the preceding proof indicates, the adiabatic method guarantees convergence of the free energy profile in Eq. (18) assuming only that the adiabatic dynamics is ergodic. As indicated in Ref. 11, such stepwise methods may miss important contributions to the free energy, particularly in the barrier region.

III. MODEL PROBLEMS AND RESULTS

In this section, the AFED method will be tested on three model problems. The first is a simple two-variable problem for which the free energy profile can be solved analytically. Here, a comparison of several different thermostating schemes will be made. The second is a simple isomerization reaction in a Lennard-Jones solvent, which serves as a paradigm for solution phase chemical processes. Here, the AFED method will also be compared to the ‘‘blue moon ensemble’’ approach based on constrained molecular dynamics.^{15,16} The third is a study of the conformational changes and corresponding free energy profile associated with the dihedral angle motion in united-atom models of butane and pentane.³² In the latter case, it will be shown that the full dihedral angle free energy *surface* can also be efficiently generated, and comparisons with a new variable transformation scheme recently introduced by us²¹ will be made. These examples serve as a paradigm for conformational equilibria in long chain molecules and in proteins. (Various other ‘‘advanced’’ methods for computing free energy profiles of rare events have recently been introduced,^{17–20} however, a detailed comparison of these methods and the present adiabatic method, although interesting, would constitute an extensive study that is beyond the scope of this paper.) All AFED free energy profiles are processed using a 11 point Savitsky–Golay filter.³³ In the context of these examples, it will be shown that free energy surfaces can also be generated efficiently.

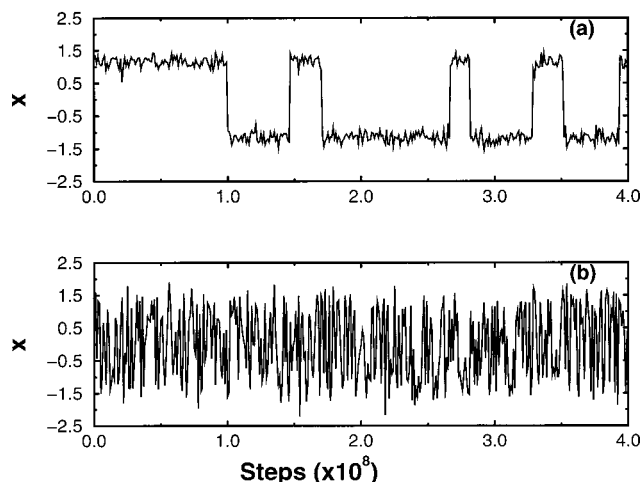


FIG. 1. Trajectory of x as a function of the number of steps for a double well coupled to a harmonic oscillator in Eq. (19). (a) Standard molecular dynamics; (b) Adiabatic (AFED) dynamics with $m_x=300$ and $T_x=10$.

A. One-dimensional quartic double well coupled to a harmonic oscillator

Consider a simple two-variable system described by the Hamiltonian in Eq. (3) with a potential of the form,

$$V(x,y) = D_0(x^2 - a^2)^2 + \frac{1}{2}\kappa y^2 + \lambda xy. \quad (19)$$

For this simple problem, $Z_y(x; \beta_y)$ can be calculated analytically, leading to a symmetric free energy profile in x given by

$$F(x) = -\frac{1}{\beta_y} \ln Z_y(x; \beta_y) = D_0(x^2 - a^2)^2 - \frac{\lambda^2}{2\kappa} x^2. \quad (20)$$

Simulations of this model system were carried out using $D_0=5$, $a=1$, $\kappa=1$, $\lambda=2.878$, $m_y=1$, and $kT_y=1$. With these parameters, the free energy profile in x has two wells located at $x_{\pm} = \pm \sqrt{a^2 + \lambda^2/4D_0\kappa} = \pm 1.189$ and a barrier at $x=0$. In addition, the free energy barrier is $F^{\ddagger} = F(x=0) - F(x_{\pm}) = D_0a^4 + \lambda^2a^2/2\kappa + \lambda^4/16D_0\kappa^2 \approx 10$.

In order to ensure efficient barrier crossing, a temperature $kT_x=10$ was chosen for AFED simulations. With this choice of kT_x , the convergence of the free energy profile with m_x was tested by performing simulations with $m_x=10, 100, 300$. For these mass choices, simulations of 10^9 steps using a time step 0.25×10^{-3} were performed. Canonical sampling is obtained using the recently introduced GGMT algorithm.³⁰ It is important to note that the thermostating method can influence the efficiency of free energy calculations. The GGMT method was chosen because, as was shown in Ref. 30, it maintains good temperature control even in problems involving motion over high barriers.

Figure 1 shows the trajectory of x as a function of time for $m_x=m_y$ and $T_x=T_y$ corresponding to an ordinary dynamics simulations compared to the AFED parameters ($m_x=300$ and $T_x=10$). The figure shows that without the adiabaticity conditions, barrier crossing is a rare event as would be expected in an ordinary dynamics calculation. In contrast, the AFED dynamics case shows frequent barrier crossing and, hence, efficient sampling of the configuration space available to x . Figure 2 shows the free energy profiles obtained from the AFED simulations for the different choices

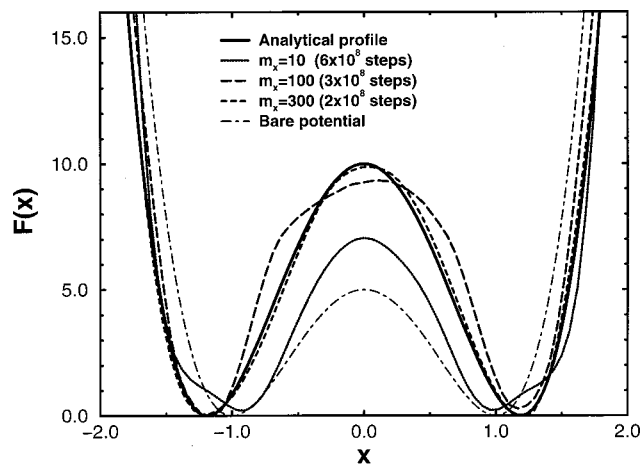


FIG. 2. Adiabatic (AFED) dynamics free energy profile for a double well coupled to a harmonic oscillator in Eq. (19). The figure shows the convergence of the free energy profile as a function of m_x with $T_x=10$. The solid line is the analytical free energy profile, the dotted line corresponds to $m_x=10$, the long dashed line corresponds to $m_x=100$, and the short dashed line corresponds to $m_x=300$. $m_y=1$ in all cases. For comparison, the bare potential is shown with the dotted-dashed line.

of m_x together with the analytical result. The figure shows that when m_x is too small, adiabaticity is not well maintained and the free energy profile is not well reproduced. It can be seen that for $m_x=300$ the agreement between the AFED and analytical results is very good (see Sec. IV for a general protocol for determining the adiabaticity control parameters, T_x and m_x). Figure 3 shows the influence of the thermostating method on the efficiency of convergence of the AFED method. In particular, a comparison is shown between the free energy profiles obtained using the widely used Nosé–Hoover chain method²⁹ to that obtained using the new GGMT approach³⁰ for runs of equal length. The figure shows that when the GGMT run is converged, the Nosé–Hoover chain method has not yet reached convergence. In this particular example, even a run length of 1.8×10^9 steps was insufficient to fully converge the free energy profile generated by the Nosé–Hoover chain method (see Fig. 3).

B. Isomerization reaction in a Lennard-Jones solvent

As a simple paradigm for solution phase chemical processes, we consider an isomerization reaction of a homonuclear diatomic molecule solvated in a Lennard-Jones (LJ) liquid. A variant of this model has been considered previously by other authors³⁴ in the context of other methodological developments. The intramolecular potential of the diatomic is characterized by a single coordinate $r = |\mathbf{r}_1 - \mathbf{r}_2|$, the distance between the two atoms comprising the diatomic. The intramolecular potential is, again, given by a quartic double well form,

$$V_{\text{intra}}(r) = D_0[(r - r_0)^2 - a^2]^2, \quad (21)$$

so that the total potential is

$$U(\mathbf{r}_1, \dots, \mathbf{r}_N) = V_{\text{intra}}(|\mathbf{r}_1 - \mathbf{r}_2|) + V_{\text{LJ}}(\mathbf{r}_1, \dots, \mathbf{r}_N), \quad (22)$$

where the LJ interaction between atoms 1 and 2 is excluded. The diatomic can exist in two stable “conformations” char-

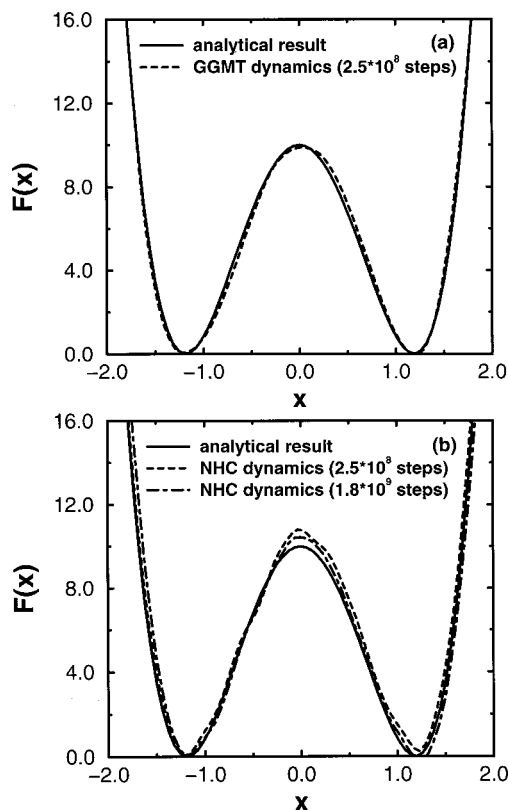


FIG. 3. The influence of the thermostating method in the calculation of the free energy profile for the harmonic oscillator linearly coupled to a double well [cf. Eq. (19)]. (a) Free energy profile generated using $m_x=300$ and $T_x=10$ with AFED dynamics using the generalized Gaussian moment thermostating (GGMT) approach (Ref. 30) and a run length of 2.5×10^8 steps (dashed line) compared to the analytical result (solid line); (b) the same comparison for AFED dynamics using the Nosé–Hoover chain thermostating approach (Ref. 29). In (b), the dotted line shows the free energy profile obtained using AFED dynamics with the Nosé–Hoover chain approach for a run length of 1.8×10^9 steps.

acterized by bond lengths $r_{\pm} = r_0 \pm a$. For this model, the free energy profile will not be symmetric about r_0 . Rather, depending on the value of r_0 , one of the two configurations will be more stable by an amount that can be determined from the free energy profile. If r_0 is large enough to allow bath particles to come between the two atoms in the molecule, the configuration with $r_0 + a$ will be stabilized, while if r_0 is small, the solvation structure around the molecule will stabilize the configuration at $r_0 - a$.

This model was simulated with different parameters. In the first case, the potential parameters are $D_0 = 10^7$ K/Å⁴, $a = 0.22$ Å, and $r_0 = 4.26$ Å. With these parameters, the stable “conformations” correspond to $r_+ = 4.48$ Å and $r_- = 4.04$ Å. The two conformations are separated by a 46.5 kcal/mol barrier at $r = r_0$ in the bare potential. The diatomic is solvated in a bath of 108 Lennard-Jones particles with $\epsilon/k = 90$ K, $\sigma = 3.405$ Å and mass $m = 39.94$ amu. The mass of the atoms in the diatomic is the same as the mass of the Lennard-Jones particles. The density and temperature of the system are $\rho\sigma^3 = 0.844$ and $T = 300$ K. In order to explore the influence of the equilibrium bond length on the free energy profile, a second case, in which r_0 was chosen to be 4.00 Å, with all the other parameters the same, was also

studied. In this case the two stable configurations occur at 3.78 Å and 4.22 Å, separated by a bare potential barrier of 46.64 kcal/mol.

In this model, the reaction coordinate is r , the diatomic bond length. The AFED method requires that the equations of motion be formulated in a coordinate system in which r is an explicit coordinate and is given both a large mass and high temperature. To see how this can be easily accomplished, consider the Lagrangian of the system,

$$L = \frac{1}{2}m(\dot{\mathbf{r}}_1^2 + \dot{\mathbf{r}}_2^2) + K_{\text{bath}} - V_{\text{intra}}(|\mathbf{r}_1 - \mathbf{r}_2|) - V_{\text{LJ}}(\mathbf{r}_1, \mathbf{r}_2, \mathbf{r}_3, \dots, \mathbf{r}_N), \quad (23)$$

where K_{bath} is the kinetic energy of the Lennard-Jones bath particles. First, we transform to center-of-mass and relative coordinates for the diatomic, $\mathbf{R} = (\mathbf{r}_1 + \mathbf{r}_2)/2$ and $\mathbf{r} = \mathbf{r}_1 - \mathbf{r}_2$, yielding

$$L = \frac{1}{2}M\dot{\mathbf{R}}^2 + \frac{1}{2}\mu\dot{\mathbf{r}}^2 + K_{\text{bath}} - V_{\text{intra}}(|\mathbf{r}|) - V_{\text{LJ}}(\mathbf{R} + \frac{1}{2}\mathbf{r}, \mathbf{R} - \frac{1}{2}\mathbf{r}, \mathbf{r}_3, \dots, \mathbf{r}_N), \quad (24)$$

where $M = 2m$ and $\mu = m/2$ are the total and reduced masses of the diatomic, respectively. Finally, we transform to spherical polar coordinates (r, θ, ϕ) in the relative coordinate giving

$$L = \frac{1}{2}M\dot{\mathbf{R}}^2 + \frac{1}{2}\mu\dot{r}^2 + \frac{1}{2}\mu r^2\dot{\mathbf{u}}^2 + K_{\text{bath}} - V_{\text{intra}}(r) - V_{\text{LJ}}(\mathbf{R} + \frac{1}{2}r\mathbf{u}, \mathbf{R} - \frac{1}{2}r\mathbf{u}, \mathbf{r}_3, \dots, \mathbf{r}_N), \quad (25)$$

where the unit vector $\mathbf{u} = (\sin\theta\cos\phi, \sin\theta\sin\phi, \cos\theta)$ is the bond orientation vector. The adiabaticity condition is imposed by choosing a temperature T_r associated with the radial degree of freedom only and by redefining the Lagrangian in Eq. (25) according to

$$L = \frac{1}{2}M\dot{\mathbf{R}}^2 + \frac{1}{2}\tilde{\mu}\dot{r}^2 + \frac{1}{2}\mu r^2\dot{\mathbf{u}}^2 + K_{\text{bath}} - V_{\text{intra}}(r) - V_{\text{LJ}}(\mathbf{R} + \frac{1}{2}r\mathbf{u}, \mathbf{R} - \frac{1}{2}r\mathbf{u}, \mathbf{r}_3, \dots, \mathbf{r}_N), \quad (26)$$

where $\tilde{\mu} \gg \mu$ is a mass associated with the r degree of freedom only.

It is important to note that, although it is necessary to work with the coordinate r explicitly, it is *not* necessary to work directly with the angular degrees of freedom θ and ϕ . Rather, we work with the Cartesian components (u_x, u_y, u_z) of the vector \mathbf{u} directly so that the kinetic energy term involving \mathbf{u} becomes

$$\frac{1}{2}\mu r^2\dot{\mathbf{u}}^2 = \frac{1}{2}\mu r^2(u_x^2 + u_y^2 + u_z^2). \quad (27)$$

When this is done, the equations of motion generated by Eq. (26) will be in terms of r and the three Cartesian components of \mathbf{u} . In order to ensure that \mathbf{u} remains a unit vector as the system evolves in time, it is necessary to add a simple constraint to the equations of motion that $u_x^2 + u_y^2 + u_z^2 = 1$. Details of how the equations of motion are integrated and how the constraint is implemented are given in Appendix B.

For $r_0 = 4.26$, AFED simulations were carried out using temperatures $T_r = 200T = 60000$ K and $T_r = 30T = 9000$ K. At $T_r = 200T$, masses of $m_r \equiv \tilde{\mu} = 3000m \approx 120 \times 10^3$ amu and $m_r = \tilde{\mu} = 6000m \approx 240 \times 10^3$ amu were used with a time step of $\Delta t = 5$ fs. At $T_r = 30T$, masses of $m_r \equiv \tilde{\mu} = 300m$

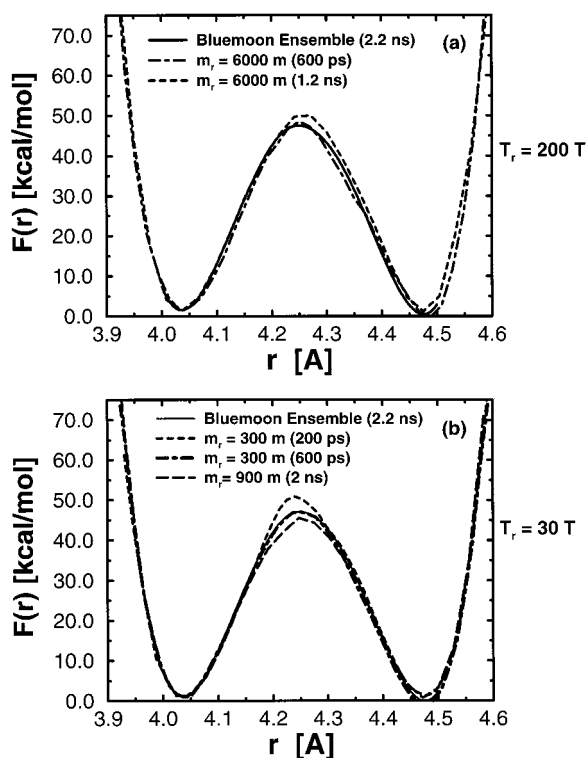


FIG. 4. Adiabatic dynamics free energy profile for an isomerizing diatomic with equilibrium bond length $r_0 = 4.26$ Å, in a Lennard-Jones solvent described in Sec. III (B). The reaction coordinate is the distance between the two atoms. The figure shows the convergence as a function of the mass \tilde{m} [cf. Eq. (26)] with $T_r = 200T = 60000$ K (a) and for $T_r = 30T = 9000$ K (b). In both panels, the solid line is the free energy profile obtained employing the “blue moon ensemble” method (Refs. 15, 16). In all cases $m = 39.94$ amu and the temperature and density are $T = 300$ K and $\rho\sigma^3 = 0.84$, respectively.

$= 11984$ amu and $m_r \equiv \tilde{m} = 900m = 35953$ amu were used. In addition, blue moon ensemble simulations were carried out using 11 evenly spaced fixed values of r between 4.0 Å and 4.50 Å (this was found to be the minimum number of points needed to generate an accurate free energy profile in this range). Each blue moon simulation consisted of 2×10^4 steps with a time step of $\Delta t = 10$ fs for a total run time of 2.2 ns. Although this is slightly longer than is actually needed to generate the free energy profile via the blue moon ensemble method, such a long run ensures a highly converged free energy profile against which the AFED method can be benchmarked. In Fig. 4, the free energy profiles obtained from the AFED calculations for the various mass and temperature choices and that obtained from the blue moon calculation are shown. It can be seen that for $T_r = 200T$ and $m_r \equiv \tilde{m} = 240 \times 10^3$ amu, the agreement between the two methods is good as well as for $T_r = 30T$ and $m_r \equiv \tilde{m} = 300m = 11984$ amu. In the former case, at $m_r = 6000m$ a 600 ps run is sufficient to converge the free energy profile, as is shown in Fig. 4(a). In the latter case, a 600 ps run yields good agreement for $m_r = 300m$, however, even a 200 ps run reproduces the free energy barrier to within about 5%. For $m_r = 900m$, a 600 ps run is insufficiently long to converge the free energy profile, however, as can be seen in Fig. 4(b), if the trajectory is allowed to run for 2 ns, it is found that the correct free energy profile is obtained. The free energy pro-

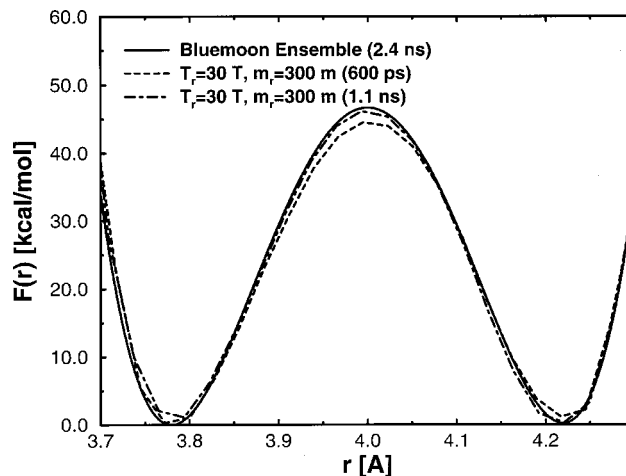


FIG. 5. Adiabatic dynamics free energy profile for an isomerizing diatomic with equilibrium bond length $r_0 = 4.00$ Å, in a Lennard-Jones solvent as described in Sec. III B. The reaction coordinate is the distance between the two atoms. The figure shows the AFED profile generated using $T_r = 30T$ and corresponding mass $m_r = 11984$ amu. For comparison, the free energy profile obtained using the blue moon ensemble approach is also shown.

files show that, at this bond length, the stable conformation at r_+ is favored by approximately 1.1 kcal/mol.

In order to compare the efficiency of the AFED and blue moon methods, the following analysis was carried out. First, note in Fig. 4, that the AFED method actually generates a larger range of r than the blue moon method. Of course, the blue moon method can be made to sample the same range of r by carrying out more simulations. In this case, 22 evenly spaced points would be required, hence, 22 simulations. Next, an AFED simulation using 22 bins for the histogram of $P(r)$ was carried out, and the error bar on the force F_r on r in one of the bins computed and compared to the error bar obtained from the blue moon ensemble method for the same value of r . It was found that, in order to obtain an error bar of size 8×10^{-5} a.u., an AFED simulation of 880 ps was needed compared to a blue moon calculation of 80 ps using the same timestep in both cases. However, since one AFED simulation generates the full free energy profile, while 22 individual blue moon simulations are needed, the total simulation time for the blue moon method would then be 22×80 ps = 1.76 ns. Thus, comparing the total simulation times, shows that the AFED method is nearly twice as efficient as the blue moon method for this example. In practice, one might be content with a restricted range for the reaction coordinate in the blue moon method. In the present example, the above analysis shows that, in this case, the two methods are, then, of equal efficiency, however, the AFED method gives a more complete picture of the free energy profile.

For $r_0 = 4.00$ Å, AFED simulations using temperatures $T_r = 30T$ with mass of $m_r \equiv \tilde{m} = 300m = 11984$ amu, and temperatures $T_r = 200T$, $T_r = 400T$ with mass of $m_r \equiv \tilde{m} = 240 \times 10^3$ amu were performed. The free energy profiles obtained with the AFED method were compared with the result of the blue moon ensemble. In this case, the blue moon simulations were carried out using 12 evenly spaced fixed values of r between 3.70 Å and 4.30 Å. The results are shown in Fig. 5. Again, it can be seen that good convergence (within 5%) is

obtained for $T_r=30T$ and $m_r \equiv \tilde{\mu} = 300m$ already after 600 ps. For this case, the free energy profiles show that the stable conformation at r_- is only slightly favored by approximately 0.2 kcal/mol.

C. United-atom butane and pentane in the gas phase

In this section, butane treated within a united-atom model,³² will be used to illustrate the application of the AFED method to a more complex reaction coordinate, namely, a backbone dihedral angle. In the united-atom representation, each CH_3 or CH_2 group is treated as a single “pseudoatom” as shown schematically in Fig. 6. Letting $\mathbf{R} \equiv \{\mathbf{r}_1, \mathbf{r}_2, \mathbf{r}_3, \mathbf{r}_4\}$ denote the four pseudoatom positions in the molecule, the intramolecular potential is given by³²

$$V_{\text{intra}}(\mathbf{R}) = V_{\text{bond}}(\mathbf{R}) + V_{\text{bend}}(\mathbf{R}) + V_{\text{dihed}}(\mathbf{R}) + V_{\text{one-four}}(\mathbf{r}_1, \mathbf{r}_4), \quad (28)$$

where the separate terms are

$$\begin{aligned} V_{\text{bond}}(\mathbf{R}) &= \sum_{i=1}^{n_{\text{bond}}} \frac{1}{2} k_{\text{bond},i} (|\mathbf{b}_i| - b_{0,i})^2, \\ V_{\text{bend}}(\mathbf{R}) &= \sum_{i=1}^{n_{\text{bend}}} \frac{1}{2} k_{\text{bend},i} (\theta_i - \theta_{0,i})^2, \\ V_{\text{dihed}}(\mathbf{R}) &= \sum_{i=1}^{n_{\text{dihed}}} C \cos(A \phi_i + \delta), \\ V_{\text{one-four}}(\mathbf{r}_1, \mathbf{r}_4) &= \sum_{i=1}^{n_{\text{one-four}}} 4\epsilon \left[\left(\frac{\sigma}{|\mathbf{r}_i - \mathbf{r}_{i+3}|} \right)^{12} - \left(\frac{\sigma}{|\mathbf{r}_i - \mathbf{r}_{i+3}|} \right)^6 \right], \end{aligned} \quad (29)$$

where $\mathbf{b}_i = \mathbf{r}_{i+1} - \mathbf{r}_i$, $\cos \theta_i = \mathbf{b}_{i+1} \cdot \mathbf{b}_i / (|\mathbf{b}_{i+1}| |\mathbf{b}_i|)$, and $\phi = \phi(\mathbf{R})$ is the dihedral angle. The potential parameters are as follows: For the $\text{CH}_3\text{-CH}_2$ and $\text{CH}_2\text{-CH}_2$ bonds, the equilibrium bond lengths are 1.54 Å and 1.52 Å, respectively, and the force constant for both bonds is $k_{\text{bond}} = 226570 \text{ K}/\text{Å}^2$; for the $\text{CH}_3\text{-CH}_2\text{-CH}_2$ bend, $\theta_0 = 111^\circ$ and $k_{\text{bend}} = 45314 \text{ rad}/\text{Å}^2$; for the dihedral angle, $C = 805.6 \text{ K}$, $A = 3$, and $\delta = 180^\circ$; for the one-four interaction between the two CH_3 pseudoatoms, $\epsilon/k = 50.35 \text{ K}$, and $\sigma = 3.385 \text{ Å}$. In order to apply the AFED method to the dihedral angle, it is necessary to transform to a coordinate frame in which ϕ is an explicit coordinate. A simple scheme for performing this transformation is given in Appendix C. Once the transformation is applied, a high temperature and large mass are assigned to the dihedral angle, thus ensuring an adiabatic separation between this degree of freedom and the remaining degrees of freedom in the system, and an adiabatic Hamiltonian is constructed as described in Appendix A [cf. Eq. (A12)].

AFED simulations of butane were carried out using temperatures $T_\phi = 5T = 1500 \text{ K}$ and $T_\phi = 10T = 3000 \text{ K}$. At $T_\phi = 5T = 1500 \text{ K}$, masses of $m_\phi = 5m = 75 \text{ amu}$, $m_\phi = 10m = 150 \text{ amu}$ and of $m_\phi = 100m = 1500 \text{ amu}$ were used. At $T_\phi = 10T = 3000 \text{ K}$, masses of $m_\phi = 10m = 150 \text{ amu}$ and of m_ϕ

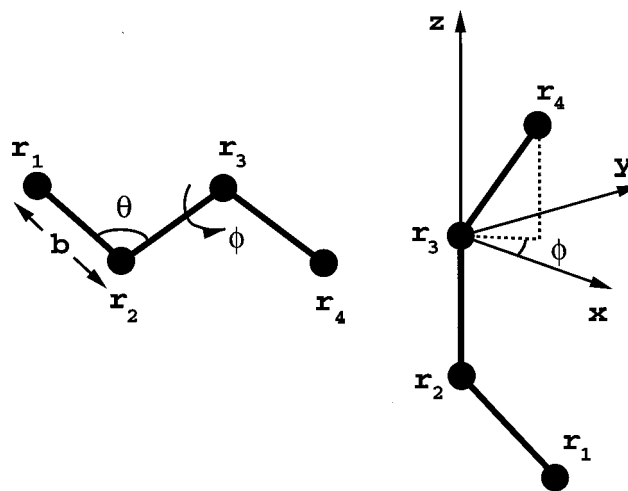


FIG. 6. United-atom representation of butane, in which each of the CH_2 and CH_3 groups are treated as “pseudoatoms.” The right panel shows that, in a particular coordinate frame, the azimuthal angle of the vector $\mathbf{r}_3 - \mathbf{r}_4$ corresponds exactly to the dihedral angle.

$= 100m = 1500 \text{ amu}$ were used. The simulation time step was $\Delta t = 0.5 \text{ fs}$ in all runs. The profiles are compared against the blue moon ensemble result. In order to perform the blue moon ensemble result, simulations were performed at 18 evenly spaced values between 0 and 2π of the dihedral angle in the generalized coordinates frame. This avoids the need to constrain the dihedral angle explicitly. Each blue moon simulation was carried out with a time step of $\Delta t = 0.2 \text{ fs}$ for a total time of 1.26 ns in order to obtain a very accurate profile against which to compare. Figure 7 shows the free energy profiles obtained from AFED simulations for different choices of the mass parameter, m_ϕ . It can be seen that for $T_\phi = 5T = 1500 \text{ K}$ good agreement with the blue moon result is obtained for a run of length 800 ps.

Once again, the relative efficiency of the AFED and blue moon methods was analyzed in a manner similar to that of Sec. III B. Thus, an AFED simulation using 18 bins for the

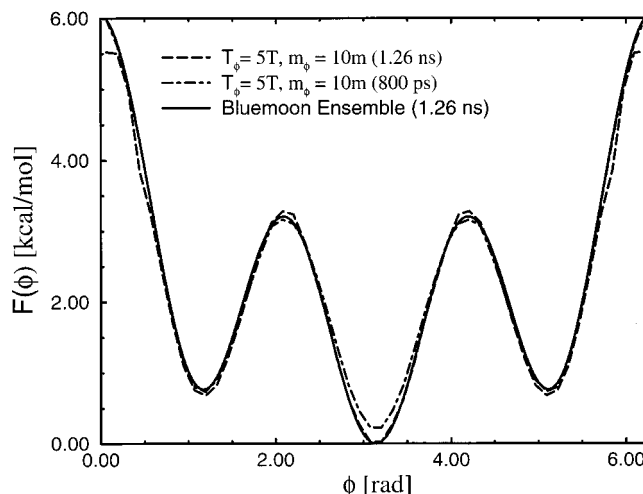


FIG. 7. Free energy profiles of the dihedral angle in united-atom butane generated using the AFED approach using $m_\phi = 5m = 75 \text{ amu}$ and $T_\phi = 5T = 1500 \text{ K}$ compared with the blue moon ensemble approach.

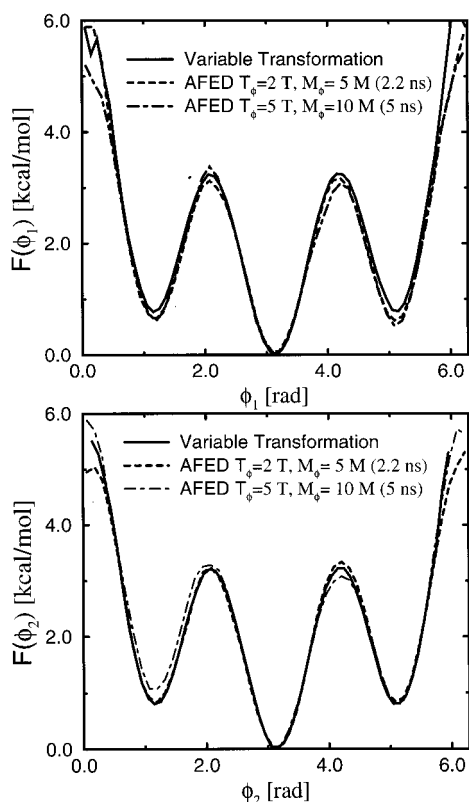


FIG. 8. Free energy profiles of the dihedral angle in united-atom pentane generated using the AFED approach using $m_\phi = 5m = 75$ amu and $T_\phi = 2T = 600$ K, $m_\phi = 10m = 150$ amu and $T_\phi = 5T = 1500$ K. (a) The C_1 - C_2 - C_3 - C_4 dihedral angle profiles; (b) the C_2 - C_3 - C_4 - C_5 dihedral angle profiles. In both cases, comparison is made to the recently introduced variable transformation approach of Zhu *et al.* (Ref. 21).

histogram was carried out and the error bar on the force F_ϕ was calculated for both methods for the same value of ϕ . In so doing, it is found that error bars of comparable sizes were obtained for the AFED and blue moon methods for runs of length 600 ps and 65 ps, respectively. The blue moon method requires 18 such simulations, while AFED only requires one, so the total length of 18 runs in the case of the former would be 1.17 ns. Comparing this number to 600 ps for the AFED simulation, it is concluded that the AFED method is roughly twice as efficient as the blue moon approach.

In order to test the ability of the AFED method to generate free energy surfaces, the example of united-atom pentane was chosen. Here, the two dihedral angles are treated as reaction coordinates which must be adiabatically decoupled from the remaining degrees of freedom in the system. Using the values $T_\phi = 2T = 600$ K, $m_\phi = 5m = 75$ amu and $T_\phi = 5T = 1500$ K and $m_\phi = 10m = 150$ amu and all other parameters the same as in the butane example, both the two one-dimensional free energy profiles of the two dihedral angle, $F(\phi_1)$ and $F(\phi_2)$ and the two-dimensional free energy surface $F(\phi_1, \phi_2)$ were generated using a single run for each set of parameters. The results are shown in Figs. 8 and 9, respectively. In Fig. 8, it can be seen that both one-dimensional free energy profiles are generated accurately using either parameter set. Here, the comparison is made to a variable transformation based scheme recently introduced by

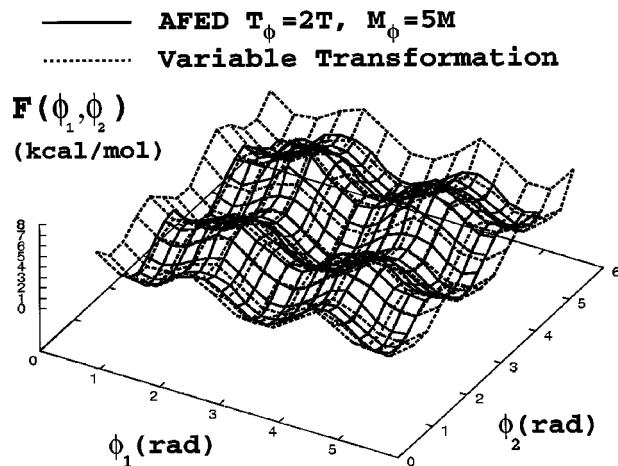


FIG. 9. Free energy surface of the two dihedral angles in united-atom pentane generated using the AFED approach with $m_\phi = 5m = 75$ amu and $T_\phi = 2T = 600$ K compared to that generated using the variable transformation approach of Zhu *et al.* (Ref. 21). For the AFED method, the surface was generated using a run length of 2.2 ns.

Zhu, Tuckerman, and Martyna,²¹ which also yields accurate free energy profiles. In Fig. 9, it is shown that the full free energy surface of the two dihedral angles is accurately generated, again using a comparison to the variable transformation method. It is important to note that the full surface can be generated with the AFED method using a simulation length no longer than that which is needed to converge a single dihedral angle distribution function, i.e., 2.2 ns in this case. By contrast, methods such as the blue moon and umbrella sampling approaches require an $N \times N$ grid in the angle space, where N is the number of points needed to perform an accurate sampling of one of the angles. Thus, the scaling of these methods would be N^2 for a surface (and, generally, N^d for a d -dimensional free energy surface). Thus, the scaling of the AFED method appears to be superior for the generation of higher dimensional free energy surfaces.

IV. DISCUSSION: CHOOSING THE ADIABATICITY PARAMETERS

In this section, a protocol for choosing the parameters for the reaction coordinate temperature and mass in order to ensure that adiabaticity is maintained and that phase space is properly sampled will be discussed. The temperature of the reaction coordinate needs to be high enough to permit activated barrier crossing on the bare potential surface, however, as Fig. 4 shows, it is possible for the value to be somewhat less than actual barrier height divided by Boltzmann's constant. In cases where free energy barriers are expected to be higher than the bare potential barrier, a larger temperature will likely be needed. In general, higher temperatures work as well but require higher masses. The mass of the reaction coordinate, which controls the adiabaticity, needs to be chosen such that the characteristic frequency of the reaction coordinate motion is small compared to that of the remaining degrees of freedom (see discussion in Sec. II). In order to determine whether a given choice of parameters leads to adiabatic dynamics, it is useful to study the velocity autocorrelation function of the two subsystems. Figure 10 shows the

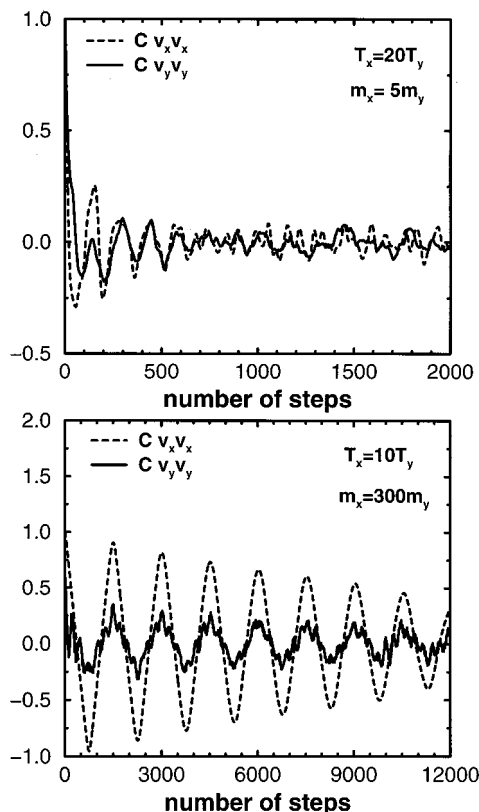


FIG. 10. Velocity autocorrelation functions $C_{v_x v_x}(t)$ and $C_{v_y v_y}(t)$ for the model x - y system defined by Eq. (19) for a “poor” choice of adiabaticity parameters ($m_x = 5m_y$ and $T_x = 20T_y$) (a) and for a good choice of adiabaticity parameters ($m_x = 300m_y$ and $T_x = 10T_y$) (b).

x and y velocity autocorrelation functions, $C_{v_x v_x}(t)$ and $C_{v_y v_y}(t)$, where $v_x = \dot{x} = p_x/m_x$ and $v_y = \dot{y} = p_y/m_y$, for the model system studied in Sec. III A for two different choices of the parameters. Figure 10(a) depicts the velocity autocorrelation functions for a “poor” choice of parameters, i.e., a choice that does not provide an adequate adiabatic decoupling of the two degrees of freedom, while Fig. 10(b) depicts these functions for a choice of parameters that does lead to adiabatic decoupling. Figure 10(b) shows that, when the dynamics is adiabatic, the motion of x and y are strongly correlated, with the long time scale of y following the single characteristic time scale of x . The short time scale of y arises from the harmonic potential contribution $\kappa y^2/2$ [cf. Eq. (19)]. This correlation is completely absent in Fig. 10(a), which corresponds to the nonadiabatic case. Note that once a mass scale separation for the reaction coordinate is chosen, the time scale for the evolution of the dynamical thermostats needs to be adjusted accordingly (see Refs. 29 and 30).

V. CONCLUSION

Given the importance of free energy calculations in the study of rare events, it is crucial to develop novel and efficient methods for computing free energy profiles along reaction paths. In this paper, a new approach to the determination of free energy profiles has been introduced. The method is based on the creation of an adiabatic separation between the reaction coordinate and the remaining degrees of freedom

within a molecular dynamics simulation. In addition, the reaction coordinate is maintained at a high temperature relative to the remaining degrees of freedom. In this way, the full configuration space corresponding to the rare event is sampled and the free energy profile is rigorously generated directly from the probability distribution of the reaction coordinate. It has been rigorously shown that the dynamics leads to a simple expression for the free energy profile in terms of the probability distribution function of the reaction coordinate. Thus, the new method requires no biasing of the configuration space, hence, no postprocessing of the output data, and leads to a scheme that is more efficient than methods based on constraining (or restraining) the reactive degree of freedom. It has also been shown that the AFED method is capable of generating free energy surfaces with an efficiency that does not scale as a power of the number of dimensions of the surface.

The new AFED method can be employed in any situation to which other free energy methods can be applied. In particular, in complex biomolecular applications, it offers several advantages in addition to increased efficiency. First, it requires no “by-hand” adjustments of the reaction coordinate. Such adjustments, usually needed in the blue moon ensemble and umbrella sampling methods, can often be difficult to perform for complex reaction coordinates and/or reaction coordinates that are strongly coupled to other degrees of freedom. A good example is that of one or more internal dihedral angle(s).

Clearly, it is not always possible to identify a useful reaction coordinate subspace however, when a useful set of reaction coordinates exists, as is often the case, the present approach has many desirable features. In addition, it is now easy to see how the AFED method can be extended to treat other types of free energy calculations, such as solvation and binding free energies or empirical valence bond approaches to charge transfer reactions.^{5,6,11} Specifically, by introducing potentials $U_A(\mathbf{r}_1, \dots, \mathbf{r}_N)$ and $U_B(\mathbf{r}_1, \dots, \mathbf{r}_N)$, corresponding to initial and final states A and B, respectively, a parameter, λ , and a generalized potential $U_\lambda(\mathbf{r}_1, \dots, \mathbf{r}_N)$ such that $U_0 = U_A$ and $U_1 = U_B$, then by introducing a momentum p_λ and a mass, m_λ , one would define an extended Hamiltonian involving the potential U_λ and an additional kinetic energy term $p_\lambda^2/2m_\lambda$. In this way, an adiabatic dynamics for λ can be constructed such that the switching between the two thermodynamic states is achieved directly without using thermodynamic integration. We are currently developing such a technique.³⁵ It is also expected that such an adiabatic approach could be combined with transition path sampling²⁻⁴ to yield a method for adiabatically generating harvestable trajectories, another application that we are currently considering. Finally, we are extending the AFED method to the computation of free energies in the isothermal–isobaric (NPT) ensemble and to the calculation of quantum free energies in both the canonical and isothermal–isobaric³⁶ ensembles via the Feynman path integral using path integral molecular dynamics techniques.^{37,38,36}

ACKNOWLEDGMENTS

This work has been funded by Research Corporation No. RI0218, NSF CHE-98-75824, and an NYU Whitehead Fellowship in biomedical and biological sciences.

APPENDIX A: TREATING AN N -PARTICLE SYSTEM IN GENERALIZED COORDINATES

In this appendix, the problem of treating an N -particle system in a set of generalized coordinate that explicitly contains the reaction coordinate is considered. From a dynamical point of view, if one begins with the Lagrangian in Cartesian coordinates, $\mathbf{r}_1, \dots, \mathbf{r}_N$,

$$L = \sum_{i=1}^N \frac{1}{2} m_i \dot{\mathbf{r}}_i^2 - V(\mathbf{r}_1, \dots, \mathbf{r}_N), \quad (\text{A1})$$

then, under a transformation to generalized coordinates q_1, \dots, q_{3N} ,

$$\begin{aligned} q_1 &= q_1(\mathbf{r}_1, \dots, \mathbf{r}_N) \\ &\dots \end{aligned} \quad (\text{A2})$$

$$q_{3N} = q_{3N}(\mathbf{r}_1, \dots, \mathbf{r}_N),$$

the Lagrangian becomes

$$L = \sum_{\alpha, \beta=1}^{3N} \frac{1}{2} G_{\alpha\beta}(q) \dot{q}_\alpha \dot{q}_\beta - V(\mathbf{r}_1(q), \dots, \mathbf{r}_N(q)), \quad (\text{A3})$$

where $q \equiv \{q_1, \dots, q_{3N}\}$ denotes the full set of generalized coordinates, and $G_{\alpha\beta}(q)$ is given by

$$G_{\alpha\beta}(q) = \sum_{i=1}^{3N} m_i \left(\frac{\partial \mathbf{r}_i}{\partial q_\alpha} \right) \cdot \left(\frac{\partial \mathbf{r}_i}{\partial q_\beta} \right) \quad (\text{A4})$$

is the mass-metric tensor. By performing the Legendre transform, the Hamiltonian can be shown to be

$$H = \frac{1}{2} \sum_{\alpha, \beta=1}^{3N} K_{\alpha\beta}(q) p_\alpha p_\beta + V(\mathbf{r}_1(q), \dots, \mathbf{r}_N(q)), \quad (\text{A5})$$

where

$$K_{\alpha\beta}(q) = \sum_{i=1}^N \frac{1}{m_i} \left(\frac{\partial q_\alpha}{\partial \mathbf{r}_i} \right) \cdot \left(\frac{\partial q_\beta}{\partial \mathbf{r}_i} \right) \quad (\text{A6})$$

is the inverse of $G_{\alpha\beta}$. The introduction of coordinate-dependent mass-metric factors into the Lagrangian/Hamiltonian of a system via a transformation to generalized coordinates leads to a considerable increase in complexity in the description of the true dynamics of the system.

Although the AFED method requires that generalized coordinates be used, the dynamics only needs to generate the correct configurational averages, and, hence, it is not necessary to work with correct conjugate momenta and the true adiabatic dynamics. This fact leads to a large simplification in the analysis and implementation of the method. In order to show this, consider the canonical partition function of the system. In Cartesian coordinates, this is given by

$$\begin{aligned} Q(N, V, T) &= \frac{1}{N! h^{3N}} \int d^N \mathbf{p} d^N \mathbf{r} \\ &\times \exp \left[-\beta \left(\sum_{i=1}^N \frac{\mathbf{p}_i^2}{2m_i} + V(\mathbf{r}_1, \dots, \mathbf{r}_N) \right) \right]. \end{aligned} \quad (\text{A7})$$

If the coordinate integration only is transformed according to Eq. (A2), leaving the momentum integrals unchanged, the partition function picks up a Jacobian factor according to

$$\begin{aligned} Q(N, V, T) &= \frac{1}{N! h^{3N}} \int d^N \mathbf{p} d^{3N} q J(q) \\ &\times \exp \left[-\beta \left(\sum_{i=1}^N \frac{\mathbf{p}_i^2}{2m_i} + V(\mathbf{r}_1(q), \dots, \mathbf{r}_N(q)) \right) \right] \\ &= \frac{1}{N! h^{3N}} \int d^N \mathbf{p} d^{3N} q \\ &\times \exp \left[-\beta \left(\sum_{i=1}^N \frac{\mathbf{p}_i^2}{2m_i} + V(\mathbf{r}_1(q), \dots, \mathbf{r}_N(q)) \right) \right. \\ &\quad \left. - \frac{1}{\beta} \ln J(q) \right]. \end{aligned} \quad (\text{A8})$$

Defining an effective potential according to

$$\begin{aligned} \tilde{V}(q_1, \dots, q_{3N}; \beta) &= V(\mathbf{r}_1(q), \dots, \mathbf{r}_N(q)) \\ &\quad - \frac{1}{\beta} \ln J(q_1, \dots, q_{3N}), \end{aligned} \quad (\text{A9})$$

the partition function becomes

$$\begin{aligned} Q(N, V, T) &= \frac{1}{N! h^{3N}} \int d^N \mathbf{p} d^{3N} q \\ &\times \exp \left[-\beta \left(\sum_{i=1}^N \frac{\mathbf{p}_i^2}{2m_i} + \tilde{V}(q_1, \dots, q_{3N}) \right) \right]. \end{aligned} \quad (\text{A10})$$

It is, thus, clear that the phase space distribution function in Eq. (A10) can be generated via molecular dynamics with a Hamiltonian of the form,

$$H = \sum_{i=1}^N \frac{\mathbf{p}_i^2}{2m_i} + \tilde{V}(q_1, \dots, q_{3N}), \quad (\text{A11})$$

where the $3N$ Cartesian momenta are treated as ‘‘conjugate’’ to the qs even though they are not the true conjugate momenta. Similarly, if q_1 is a reaction coordinate of interest, then the AFED method can be implemented by introducing a temperature T_1 for this variable and writing the Hamiltonian in the form,

$$H = \frac{p_1^2}{2\tilde{m}_1} + \sum_{\alpha=2}^{3N} \frac{p_\alpha^2}{2m_\alpha} + \tilde{V}(q_1, \dots, q_{3N}), \quad (\text{A12})$$

where $m_1 \gg m_\alpha$, $\alpha = 2, \dots, 3N$, in order to ensure an adiabatic separation. Under these conditions, the analysis of Sec. II can be applied to a general N -particle system in generalized coordinates with no modification except for a simple replacement of the N -particle potential V with the modified potential

\tilde{V} . The Hamiltonian in Eq. (A12) will not generate the true adiabatic dynamics, however, it will generate a correct sampling of the configuration space and produce the correct free energy profile (see discussion in Sec. II). It should be noted that, under certain conditions, it may be straightforward to work in terms of a full canonical set of generalized coordinates, such as in the example of Sec. III B.

APPENDIX B: A SIMPLE, REVERSIBLE INTEGRATOR FOR TREATING A DISTANCE AS A REACTION COORDINATE

In this appendix, the implementation of the AFED method for the isomerization reaction of Sec. III B is discussed. The procedure presented here is generally applicable to any problem for which the reaction coordinate is a distance. As seen in Sec. III B the Lagrangian of the system can be rewritten as

$$L = \frac{1}{2}M\dot{\mathbf{R}}^2 + \frac{1}{2}\tilde{\mu}\dot{r}^2 + \frac{1}{2}\mu r^2\dot{\mathbf{u}}^2 + K_{\text{bath}} - V_{\text{intra}}(r) - V_{\text{LJ}}(\mathbf{R} + \frac{1}{2}r\mathbf{u}, \mathbf{R} - \frac{1}{2}r\mathbf{u}, \mathbf{r}_3, \dots, \mathbf{r}_N), \quad (\text{B1})$$

where r , the bond length, is the reaction coordinate, \mathbf{u} is the unit vector along the bond, K_{bath} is the kinetic energy of the bath, and $\tilde{\mu} \gg \mu$ is a mass associated with the r degree of freedom only. In addition, $F_r = -V'_{\text{intra}}(r) - \partial V_{\text{LJ}}/\partial r$ and $\mathbf{F}_{\mathbf{u}} = -\partial V_{\text{LJ}}/\partial \mathbf{u}$. From Eq. (B2), the equations of motion for r and \mathbf{u} follow directly,

$$\begin{aligned} \dot{r} &= v_r, \\ \dot{\mathbf{u}} &= \mathbf{v}_{\mathbf{u}}, \\ \dot{v}_r &= \frac{\mu}{\tilde{\mu}} r \mathbf{v}_{\mathbf{u}}^2 + \frac{1}{\tilde{\mu}} F_r, \\ \dot{\mathbf{v}}_{\mathbf{u}} &= -\frac{2}{r} v_r \mathbf{v}_{\mathbf{u}} + \frac{1}{\mu r^2} \mathbf{F}_{\mathbf{u}}. \end{aligned} \quad (\text{B2})$$

The equations of motion, Eqs. (B2), are slightly more complicated than the usual equations of motion encountered in ordinary molecular dynamics, and, therefore, the problem of constructing a reversible, symplectic integrator for them based on the Liouville operator formalism is discussed below.

The Liouville operator corresponding to Eqs. (B2) is

$$\begin{aligned} iL &= iL_1 + iL_2 + iL_3, \\ iL_1 &= v_r \frac{\partial}{\partial r} + \mathbf{v}_{\mathbf{u}} \cdot \frac{\partial}{\partial \mathbf{u}}, \\ iL_2 &= \left(\frac{F_r}{\tilde{\mu}} + \frac{\mu}{\tilde{\mu}} r \mathbf{v}_{\mathbf{u}}^2 \right) \frac{\partial}{\partial v_r}, \\ iL_3 &= \left(-\frac{2}{r} v_r \mathbf{v}_{\mathbf{u}} + \frac{1}{\mu r^2} \mathbf{F}_{\mathbf{u}} \right) \cdot \frac{\partial}{\partial \mathbf{v}_{\mathbf{u}}}. \end{aligned} \quad (\text{B3})$$

In order to generate a reversible integrator for Eqs. (B2), the following factorization of the classical propagator, $\exp(iL\Delta t)$ for a time step, Δt is constructed:

$$\begin{aligned} \exp(iL\Delta t) &\approx \exp\left(iL_2 \frac{\Delta t}{4}\right) \exp\left(iL_3 \frac{\Delta t}{2}\right) \exp\left(iL_2 \frac{\Delta t}{4}\right) \\ &\quad \times \exp(iL_1 \Delta t) \exp\left(iL_2 \frac{\Delta t}{4}\right) \\ &\quad \times \exp\left(iL_3 \frac{\Delta t}{2}\right) \exp\left(iL_2 \frac{\Delta t}{4}\right). \end{aligned} \quad (\text{B4})$$

Application of this operator to the phase space vector gives the time evolution of the variables, r , v_r , \mathbf{u} , $\mathbf{v}_{\mathbf{u}}$. The operators that act on the variables r , v_r , \mathbf{u} yield a simple time translation, while the action of $\exp(iL_3\Delta t/2)$ gives the following evolution of $\mathbf{v}_{\mathbf{u}}$:

$$\begin{aligned} \mathbf{v}_{\mathbf{u}}(\Delta t/2) &= \mathbf{v}_{\mathbf{u}}(0) \exp\left(-\frac{1}{r} v_r \Delta t\right) \\ &\quad + \frac{1}{2\mu r v_r} \left[1 - \exp\left(-\frac{1}{r} v_r \Delta t\right) \right] \mathbf{F}_{\mathbf{u}}(0), \end{aligned} \quad (\text{B5})$$

where v_r has the value it has obtained when the operator, $\exp(iL_3\Delta t/2)$ is applied. The potentially singular term, $[1 - \exp(-\Delta t/r v_r)]/v_r$, can be expanded in a Maclaurin series when v_r is small, since its limit for $v_r \rightarrow 0$ is finite.

In order to complete the scheme, it is necessary to add an additional force that constrains \mathbf{u} to be a unit vector. This is accomplished by modifying the equation of motion for \mathbf{u} according to

$$\dot{\mathbf{v}}_{\mathbf{u}} = -\frac{2}{r} v_r \mathbf{v}_{\mathbf{u}} + \frac{1}{\mu r^2} (\mathbf{F}_{\mathbf{u}} - \lambda \mathbf{u}). \quad (\text{B6})$$

In Eq. (B6), a constraint force $-\lambda \mathbf{u}$ has been added to $\mathbf{F}_{\mathbf{u}}$, where λ is a Lagrange multiplier that ensures the condition $\mathbf{u}(t) \cdot \mathbf{u}(t) = 1$ is maintained at all time t . The multiplier is calculated using the standard procedure. The vector \mathbf{u} is updated in the absence of the constraint force using Eq. (B5) to produce the unconstrained evolution $\mathbf{u}''(\Delta t)$. The vector $\mathbf{u}(\Delta t)$ is then constructed according to

$$\mathbf{u}(\Delta t) = \mathbf{u}''(\Delta t) - \lambda \frac{\Delta t^2}{2\mu r^2} \mathbf{u}(0). \quad (\text{B7})$$

Defining $\lambda' = \lambda \Delta t^2 / 2\mu r^2$, the condition $|\mathbf{u}(\Delta t)|^2 = 1$ is then imposed, which leads to the following expression for λ' :

$$\lambda' = \mathbf{u}(0) \cdot \mathbf{u}''(\Delta t) - \sqrt{|\mathbf{u}(0) \cdot \mathbf{u}''(\Delta t)|^2 - (|\mathbf{u}''(\Delta t)|^2 - 1)}. \quad (\text{B8})$$

Once the multiplier has been determined, $\mathbf{u}(\Delta t)$ is obtained from Eq. (B7), and the velocity $\mathbf{v}_{\mathbf{u}}(\Delta t/2)$ at the half-step obtained from

$$\mathbf{v}_{\mathbf{u}}(\Delta t/2) = \mathbf{v}''(\Delta t/2) - \frac{\lambda'}{\Delta t} \mathbf{u}(0). \quad (\text{B9})$$

The forces are then recalculated at the new positions, and $\mathbf{v}_{\mathbf{u}}$ is updated with the appropriate updated unconstrained force according to Eq. (B5). Finally, the constraint force is applied, and the resulting update for $\mathbf{v}_{\mathbf{u}}$, leading to the fully updated velocity is

$$\mathbf{v}_{\mathbf{u}}(\Delta t) = \mathbf{v}_{\mathbf{u}}''(\Delta t) - (\mathbf{u}(\Delta t) \cdot \mathbf{v}_{\mathbf{u}}''(\Delta t)) \mathbf{u}(\Delta t), \quad (\text{B10})$$

where $\mathbf{v}_{\mathbf{u}}''(\Delta t)$ is the velocity just before the constraint force at Δt is applied. Additionally, it is necessary to apply ther-

mostats to ensure canonical sampling. As discussed in Sec. II, a thermostat is applied to the reaction coordinate r , maintaining its temperature at an elevated value T_r . Because of the constraint on \mathbf{u} , it is necessary to thermostat the three components of \mathbf{u} together and separately from the remaining bath degrees of freedom.³⁹ Apart from this, the application of the thermostat operators follows the procedure described in detail in Refs. 29 and 39. Finally, it should be noted that the formulation of the integrator via the Liouville operator allows the AFED method to be easily combined with multiple time scale integration (RESPA) (Ref. 31) techniques for the bath.

APPENDIX C: A SIMPLE VARIABLE TRANSFORMATION SCHEME FOR TREATING A DIHEDRAL ANGLE AS A REACTION COORDINATE

Although it may seem that the need to use generalized coordinates in the AFED method is a disadvantage, it has been shown in Appendices A and B that this is less of a disadvantage than one might expect. In Appendix A, it was shown that it is only necessary to transform the coordinates and not the momenta, which considerably simplifies the problem of working in generalized coordinates. In Appendix B, a simple scheme was developed to integrate the equations of motion in spherical polar coordinates when a distance (radial) coordinate is the reaction coordinate. In addition, coordinate transformations can be used in other ways to enhance conformational sampling in molecular dynamics calculations.²¹ Here, it is shown that treating dihedral angles is also possible with relatively little effort, thus allowing for a wide range of applications for the AFED method. AFED can be implemented easily using a set of generalized coordinates which contains explicitly the dihedral angle as an explicit coordinate. Below, an algorithm for generating such a coordinate transformation is described.

It is particularly convenient to carry out the transformation in three successive steps. First, a translation of the vector \mathbf{r}_4 (see Fig. 6) to a frame in which \mathbf{r}_3 is at the origin is performed,

$$\mathbf{r}'_1 = \mathbf{r}_1, \quad \mathbf{r}'_2 = \mathbf{r}_2, \quad \mathbf{r}'_3 = \mathbf{r}_3, \quad \mathbf{r}'_4 = \mathbf{r}_4 - \mathbf{r}_3. \quad (\text{C1})$$

The coordinate frame is then rotated to a frame in which the vector $\mathbf{r}'_2 - \mathbf{r}'_3$ lies along the z -axis and the vector $(\mathbf{r}'_2 - \mathbf{r}'_3) \times (\mathbf{r}'_2 - \mathbf{r}'_1)$ lies along the y -axis,

$$\mathbf{r}''_1 = \mathbf{r}'_1, \quad \mathbf{r}''_2 = \mathbf{r}'_2, \quad \mathbf{r}''_3 = \mathbf{r}'_3, \quad \mathbf{r}''_4 = R(\mathbf{r}'_1, \mathbf{r}'_2, \mathbf{r}'_3)\mathbf{r}'_4. \quad (\text{C2})$$

The matrix, $R(\mathbf{r}'_1, \mathbf{r}'_2, \mathbf{r}'_3)$ is a rotation matrix for orienting the coordinate frame in this manner. The elements of the rotation matrix are as follows:

$$R(\mathbf{r}'_1, \mathbf{r}'_2, \mathbf{r}'_3) = \begin{pmatrix} \frac{(\mathbf{r}'_3 - \mathbf{r}'_2) \times (\mathbf{r}'_1 - \mathbf{r}'_2)}{|(\mathbf{r}'_3 - \mathbf{r}'_2) \times (\mathbf{r}'_1 - \mathbf{r}'_2)|} \times \frac{\mathbf{r}'_3 - \mathbf{r}'_2}{|\mathbf{r}'_3 - \mathbf{r}'_2|} \\ \frac{(\mathbf{r}'_3 - \mathbf{r}'_2) \times (\mathbf{r}'_1 - \mathbf{r}'_2)}{|(\mathbf{r}'_3 - \mathbf{r}'_2) \times (\mathbf{r}'_1 - \mathbf{r}'_2)|} \\ \frac{\mathbf{r}'_3 - \mathbf{r}'_2}{|\mathbf{r}'_3 - \mathbf{r}'_2|} \end{pmatrix}, \quad (\text{C3})$$

where the x , y , and z components of the three vectors constitute the rows of the matrix. When this is done, the vector \mathbf{r}''_4 is resolved into spherical polar coordinates, so that the final coordinates are

$$\begin{aligned} \mathbf{r}'''_1 &= \mathbf{r}''_1, & \mathbf{r}'''_2 &= \mathbf{r}''_2, & \mathbf{r}'''_3 &= \mathbf{r}''_3, \\ r'''_4 &= \sqrt{x_4''^2 + y_4''^2 + z_4''^2}, \\ \theta'''_4 &= \arctan(\sqrt{x_4''^2 - y_4''^2}/z_4''), \\ \phi'''_4 &= \arctan(y_4''/x_4''). \end{aligned} \quad (\text{C4})$$

The azimuthal angle, ϕ'''_4 is, then, the required dihedral angle as shown clearly in Fig. 6. Using this set of generalized coordinates, AFED simulations can be performed straightforwardly, using a Hamiltonian of the form given in Eq. (A12), by associating a high temperature and large mass with the coordinate ϕ'''_4 .

- ¹R. J. Radmer and P. A. Kollman, *J. Comput. Chem.* **18**, 902 (1997).
- ²C. Dellago, P. G. Bolhuis, F. S. Csajka, and D. Chandler, *J. Chem. Phys.* **108**, 1964 (1998).
- ³C. Dellago, P. G. Bolhuis, and D. Chandler, *J. Chem. Phys.* **110**, 6617 (1999).
- ⁴P. G. Bolhuis, C. Dellago, P. L. Geissler, and D. Chandler, *J. Phys.: Condens. Matter* **12**, A147 (2000).
- ⁵A. Warshel, *J. Phys. Chem.* **86**, 2218 (1982).
- ⁶J. K. Hwang, G. King, S. Creighton, and A. Warshel, *J. Am. Chem. Soc.* **110**, 5297 (1988).
- ⁷H. Resat and M. Mezei, *J. Chem. Phys.* **101**, 6126 (1994).
- ⁸P. V. Maye and M. Mezei, *J. Mol. Struct.: THEOCHEM* **362**, 317 (1996).
- ⁹A. Degaegere and M. Karplus, *J. Phys. Chem.* **100**, 11148 (1996).
- ¹⁰G. Hummer and A. Szabo, *J. Chem. Phys.* **105**, 2004 (1996).
- ¹¹J. Villa and A. Warshel, *J. Phys. Chem. B* **105**, 7887 (2001).
- ¹²G. M. Torrie and J. P. Valleau, *Chem. Phys. Lett.* **28**, 578 (1974).
- ¹³G. M. Torrie and J. P. Valleau, *J. Comput. Phys.* **23**, 187 (1977).
- ¹⁴J. P. Valleau and G. M. Torrie, in *Modern Theoretical Chemistry V*, edited by B. J. Berne (Plenum, New York, 1977).
- ¹⁵E. A. Carter, G. Ciccotti, J. T. Hynes, and R. Kapral, *Chem. Phys. Lett.* **156**, 472 (1989).
- ¹⁶M. Sprink and G. Ciccotti, *J. Chem. Phys.* **109**, 7737 (1998).
- ¹⁷Z. Z. Fan, J. K. Hwang, and A. Warshel, *Theor. Chem. Acc.* **103**, 77 (1999).
- ¹⁸J. VandeVondele and U. Rothlisberger, *J. Chem. Phys.* **113**, 4863 (2000).
- ¹⁹D. A. Hendrix and C. Jarzynski, *J. Chem. Phys.* **114**, 5974 (2001).
- ²⁰S. Melchionna, *Phys. Rev. E* **62**, 8762 (2000).
- ²¹Z. Zhu, M. E. Tuckerman, and G. J. Martyna, *Phys. Rev. Lett.* (in press).
- ²²S. Kumar, R. H. Swendsen, P. A. Kollman, and J. M. Rosenberg, *J. Comput. Chem.* **13**, 1011 (1992).
- ²³L. Rosso and M. E. Tuckerman, *Mol. Simul.* **28**, 91 (2002).
- ²⁴R. E. Bruccoleri and M. Karplus, *Biopolymers* **29**, 3975 (1990).
- ²⁵S. Samuelson and G. J. Martyna, *J. Chim. Phys.* **94**, 1503 (1997).
- ²⁶J. Cao and G. J. Martyna, *J. Chem. Phys.* **104**, 2028 (1996).
- ²⁷D. Marx, M. E. Tuckerman, and G. J. Martyna, *Comput. Phys. Commun.* **118**, 166 (1999).
- ²⁸R. Car and M. Parrinello, *Phys. Rev. Lett.* **55**, 2471 (1985).
- ²⁹G. J. Martyna, M. E. Tuckerman, and M. L. Klein, *J. Chem. Phys.* **97**, 2635 (1992).
- ³⁰Y. Liu and M. E. Tuckerman, *J. Chem. Phys.* **112**, 1685 (2000).
- ³¹M. E. Tuckerman, G. J. Martyna, and B. J. Berne, *J. Chem. Phys.* **97**, 1990 (1992).
- ³²J. P. Ryckaert and A. Bellemans, *Faraday Discuss.* **66**, 95 (1978).
- ³³W. H. Press, S. A. Teukolsky, W. T. Vetterling, and B. P. Flannery, *Numerical Recipes in C* (Cambridge University Press, Cambridge, 1992).
- ³⁴J. E. Straub, M. Borkovec, and B. J. Berne, *J. Chem. Phys.* **89**, 4833 (1988).
- ³⁵L. Rosso and M. E. Tuckerman (to be submitted).

³⁶G. J. Martyna, A. Hughes, and M. E. Tuckerman, *J. Chem. Phys.* **110**, 3275 (1999).

³⁷M. E. Tuckerman, G. J. Martyna, M. L. Klein, and B. J. Berne, *J. Chem. Phys.* **99**, 2796 (1993).

³⁸M. E. Tuckerman, D. Marx, M. L. Klein, and M. Parrinello, *J. Chem. Phys.* **104**, 5579 (1996).

³⁹G. J. Martyna, M. E. Tuckerman, D. J. Tobias, and M. L. Klein, *Mol. Phys.* **87**, 1117 (1996).